J Biol Inorg Chem (2016) 21:491–499
DOI 10.1007/s00775-016-1359-6

ORIGINAL PAPER

# A realistic in silico model for structure/function studies of molybdenum–copper CO dehydrogenase

**Dalia Rokhsana[1] · Tao A. G. Large[1] · Morgan C. Dienst[1] · Marius Retegan[2,3] · Frank Neese[2]**

Received: 12 November 2015 / Accepted: 5 May 2016 / Published online: 26 May 2016


**Abstract** CO dehydrogenase (CODH) is an environmentally crucial bacterial enzyme that oxidizes CO to $CO_2$ at a Mo–Cu active site. Despite the close to atomic resolution structure (1.1 Å), significant uncertainties have remained with regard to the protonation state of the water-derived equatorial ligand coordinated at the Mo-center, as well as the nature of intermediates formed during the catalytic cycle. To address the protonation state of the equatorial ligand, we have developed a realistic in silico QM model (~179 atoms) containing structurally essential residues surrounding the active site. Using our QM model, we examined each plausible combination of redox states ($Mo^{VI}$–$Cu^{I}$, $Mo^{V}$–$Cu^{II}$, $Mo^{V}$–$Cu^{I}$, and $Mo^{IV}$–$Cu^{I}$) and Mo-coordinated equatorial ligands ($O^{2-}$, $OH^{-}$, $H_2O$), as well as the effects of second-sphere residues surrounding the active site. Herein, we present a refined computational model for the Mo(VI) state in which Glu763 acts as an active site base, leading to a $MoO_2$-like core and a protonated Glu763. Calculated structural and spectroscopic data (hyperfine couplings) are in support of a $MoO_2$-like core in agreement with XRD data. The calculated two-electron reduction potential ($E = -467$ mV vs. SHE) is in reasonable agreement with the experimental value ($E = -558$ mV vs. SHE) for the redox couple comprising an equatorial oxo ligand and protonated Glu763 in the $Mo^{VI}$–$Cu^{I}$ state and an equatorial water in the $Mo^{IV}$–$Cu^{I}$ state. We also suggest a potential role of second-sphere residues (e.g., Glu763, Phe390) based on geometric changes observed upon exclusion of these residues in the most plausible oxidized states.

**Keywords** CO dehydrogenase · Molybdenum–copper bimetallic site · Density functional theory · Quantum mechanics · Computational model

## Introduction

Carbon monoxide dehydrogenase (CODH) from the aerobic soil bacterium *Oligotropha carboxidovorans* is a member of the xanthine oxidase family of molybdenum-containing enzymes. It contains a unique Mo–Cu bimetallic active site that catalyzes the conversion of CO to $CO_2$ shown in Eq. 1, removing an estimated $2 \times 10^8$ tons of CO from the lower atmosphere and soil per year [1, 2]. A recent study has revealed that CODH is also capable of splitting dihydrogen into protons and electrons [3], though this is not its main catalytic function.

$$CO + H_2O \rightarrow CO_2 + 2H^+ + 2e^- \quad E_{red}{}^{o\prime} = -558 \text{ mV at pH } 7.0 \qquad (1)$$

The CODH enzyme from *Oligotropha carboxidovorans* has been crystallized as a dimer of αβγ heterotrimers in the postulated active oxidized $Mo^{VI}$–$Cu^{I}$ (PDB ID: 1N5W) and substrate-reduced intermediate $Mo^{IV}$–$Cu^{I}$ (PDB ID: 1N63) states [4]. Each heterotrimer contains a bimetallic Mo–Cu center, a noncovalently bound flavin adenine dinucleotide (FAD) cofactor, and two [2Fe–2S] clusters. The coordination environment around the metal centers is shown in Fig. 1. Five ligands were found at the Mo-center arranged

**Electronic supplementary material** The online version of this article (doi:10.1007/s00775-016-1359-6) contains supplementary material, which is available to authorized users.

✉ Dalia Rokhsana
rokhsad@whitman.edu

[1] Department of Chemistry, Whitman College, Walla Walla, WA 99362, USA

[2] Max Planck Institute for Chemical Energy Conversion, 45470 Mülheim an der Ruhr, Germany

[3] Present Address: European Synchrotron Radiation Facility, BP 220, 38043 Grenoble Cedex, France

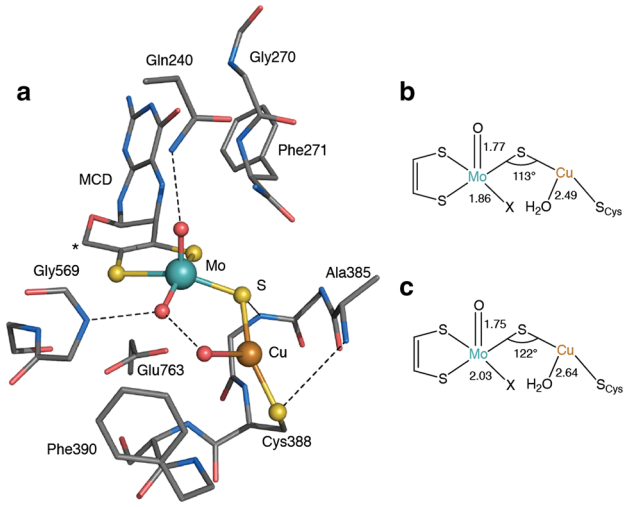


**Fig. 1** **a** Key residues contributing to the network of weak interactions about the Mo–Cu center; schematic structure of **b**, the oxidized $Mo^{VI}$–$Cu^{I}$ state (PDB ID: 1N5W, X = $O^{2-}$/$OH^{-}$), and **c**, the substrate-reduced $Mo^{IV}$–$Cu^{I}$ state (PDB ID: 1N63, X = $OH^{-}$/$H_2O$) along with selected internuclear distances (Å) and angles (°)

in a distorted square pyramidal geometry with one axial oxo ($O^{2-}$) ligand, and four equatorial ligands comprising a water-derived second oxygen ligand, two sulfur atoms from a molybdopterin cytosine dinucleotide (MCD) cofactor, and a μ-sulfido ligand. The latter links the Mo-center to the Cu-center, which is additionally coordinated by a sulfur atom from Cys388, and by a weakly coordinated $H_2O$ molecule at a distance of ~2.49 Å (Fig. 1) [4, 5].

Comparison of structural parameters for the two forms ($Mo^{VI}$–$Cu^{I}$ and $Mo^{IV}$–$Cu^{I}$) obtained from X-ray diffraction (XRD) and extended X-ray absorption fine structure (EXAFS) spectroscopic analyses revealed several disparities with respect to distances within the primary coordination environment [5]. In the oxidized state, the Mo–O distances were found to be inequivalent (1.77 and 1.86 Å) in the reported XRD data (RMSD = 0.02 Å), but were reported as equivalent (1.74 ± 0.02 Å) based on the EXAFS analysis [4]. This might be taken as evidence for the presence of two oxygen ligands that differ in protonation state between the solution and crystalline states. The discrepancy has been previously acknowledged, and has been attributed to changes in physicochemical conditions between CODH in solution (low salt, aqueous) and crystalline environments (high salt, presence of 2-methyl-2,4-pentanediol) [5]. An elongation of the Mo–$O_{eq}$ distance in XRD and EXAFS datasets was observed upon two-electron reduction of the oxidized enzyme, suggesting a possible change in the protonation state of the equatorial ligand between the catalytically relevant states as well [4, 5]. Additionally, the μS–Cu–$S_{Cys}$ bond angle increased by ~10°, and has been suggested to play a major role in modulating electronic structure by altering the orbital overlap between the copper and the sulfido ligand bridging the two metals.

The active site geometry of CODH is greatly influenced by a network of weak interactions from key second- and outer-sphere amino acid residues, as shown in Fig. 1 [4]. A conserved glutamic acid residue (Glu763) is located in close proximity to the equatorial oxygen, and is thought to act as an active site base. A phenylalanine residue (Phe390) located in a flexible loop is also conserved among xanthine oxidases, and is suggested to play a role in positioning weakly coordinated water in addition to substrates and inhibitors at the active site.

Resonance Raman provides additional support for a $MoO_2$-like coordination environment in the oxidized state of the enzyme. Two distinct Mo=O stretching modes were identified (assigned previously as $\nu_{sym.}$ = 895 $cm^{-1}$ and $\nu_{asym.}$ = 861 $cm^{-1}$) in analogy with the modes reported for the sulfite oxidase enzyme, and consistent with other molybdenum complexes containing similar $MoO_2$ cores [6]. The spectroscopic properties of the one-electron reduced species, either trapped with CO or bicarbonate-bound, were investigated using electron nuclear double resonance (ENDOR) spectroscopy. Additional features were observed in the spectrum of the dithionite-reduced enzyme, more complex than those observed for the enzyme treated with CO. Such complex features could result from proton hyperfine coupling of the coordinating ligands ($OH^{-}$ and $H_2O$) to nuclei about the bimetallic site [4–7].

Previous computational studies have used small quantum mechanics (QM) models to map out the molecular mechanism of CO conversion, resulting in the proposal of multiple mechanistic pathways [8, 9]. The uncertain protonation state of the equatorial oxygen in these catalytic states, however, has yet to be rigorously investigated. As the potentially extensive influence of H-bonding interactions and outer-sphere residues on the active site geometry is well established, we postulate that a more extensive QM model may be required to assess all plausible protonation states of the equatorial ligand. This analysis is crucial for investigating the catalytic mechanism of CO oxidation, as it could alter substantially the potential energy landscape.

To develop a sufficiently comprehensive QM model, we have investigated and included all structurally essential features of second- and outer-sphere residues surrounding the primary coordination sphere of the Mo–μS–Cu unit. All plausible ligand variations were considered at the Mo-equatorial position ($O^{2-}$, $OH^{-}$, $H_2O$), in conjunction with all plausible oxidation state combinations for the metal centers (Mo = VI, V, IV; Cu = II, I). These models were evaluated using the available experimental data, including structural parameters, vibrational frequencies, reduction potentials, *g* values, and hyperfine couplings (HFCs). Finally, to establish the structural role of individual residues surrounding the active site, models excluding key residues were reoptimized, and the

resulting structural changes observed. Here, we report our refined computational model of the CODH active site, including the most likely protonation state of the equatorial oxygen ligand coordinated to Mo, as well as insights into the influence of surrounding residues on the key geometric parameters and electronic structural features of the Mo–μS–Cu core.

## Computational details

All computational models were developed from the oxidized crystal structure (PDB ID: 1N5W) [4]. The largest model, containing ~179 atoms, included the flexible loop residues from Val384 through Phe390, along with Gln240, Glu763, Gly569, Ser570, Gly269, Gly270, Phe271, and an additional crystallographic water molecule found near the Cu-center (HOH5313) (Fig. 1). This water corresponds to the similarly positioned HOH5295 in the CO-reduced structure (1N63). The side chains of Tyr386 and Arg387 were truncated, as in the reported models. All protein residues were modeled as charge-neutral, except for Glu763 (−1) and Cys388 (−1). In the $Mo^{VI}$–$Cu^{I}$ oxidation state, the total charge of the QM model was either −3 or −2, corresponding, respectively, to an equatorial $O^{2-}$ or $OH^{-}$ ligand. Other charge states investigated for our QM model with varying Mo-equatorial ligands were as follows (charge, spin multiplicity): $Mo^{V}$–$Cu^{I}$–Oxo (−4, 2), $Mo^{V}$–$Cu^{I}$–OH (−3, 2), $Mo^{V}$–$Cu^{II}$–Oxo (−3, 3 and −3, 1), $Mo^{V}$–$Cu^{II}$–OH (−2, 3 and −2, 1), $Mo^{IV}$–$Cu^{I}$–OH (−4, 1), and $Mo^{IV}$–$Cu^{I}$–$OH_2$ (−3, 1) (Fig. 2). For the model containing an equatorial $OH^{-}$, several different H-bonding orientations were initially considered to identify the lowest energy conformer (Fig. 3).

All calculations were performed using the ORCA quantum chemistry package [10]. During geometry optimization, all αC atoms were kept frozen at the crystallographic positions along with one attached proton each (omitted for clarity), as were one C atom and one attached proton of the MCD cofactor (indicated with an asterisk in Fig. 1). Geometry optimizations were performed employing the conductor-like screening model (COSMO) [11] with a solvent dielectric constant $\varepsilon = 4.0$, using the BP86 density functional [12, 13] and the zero-order regular approximation Hamiltonian (ZORA) to account for scalar relativistic effects [14]. The ZORA-recontracted versions of the def2-TZVP basis sets were used for all elements with the exception of the hydrogen and carbon atoms, for which the basis sets were reduced to the ZORA version of def2-SVP [15]. The resolution of identity [16] with the appropriate auxiliary basis sets [17] was used to accelerate the calculations. Vibrational frequencies were calculated using the recently developed efficient implementation of the analytical second derivatives of the SCF energy [18]. Intrinsic atomic orbitals were used to assign the correct oxidation states of the metal centers [19].

Reduction potentials were calculated using the well-known relation $\Delta G^{\circ} = -nFE^{\circ}$, taking the energy differences between the oxidized and two-electron reduced states, and considering each plausible protonation state for the water-derived equatorial oxygen ligand. The energy of the system, including dispersion corrections and implicit solvent contributions, was evaluated using the same basis set and the B3LYP hybrid functional containing 20 % exact exchange [20], as hybrid functionals typically provide superior accuracy for this type of property [21]. The calculations were accelerated through the chain-of-spheres approximation [22, 23]. Variability in the solvent polarity was taken into account by considering a comprehensive range of solvent dielectric constants ($\varepsilon = 4$, 10, 15, 80) in the implicit solvent model to approximate the solvation environment around the active site. Experimental solvation energies for the water-derived proton (−264 kcal/mol, or −0.42 eV) were used in the reduction potential calculations [24]. Reduction potentials are reported relative to the reference potential of the standard hydrogen electrode (4.44 ± 0.02 V at 25 °C). The g-tensors and HFCs ($A_{Mo}$, $A_{Cu}$ and $A_{H}$) were

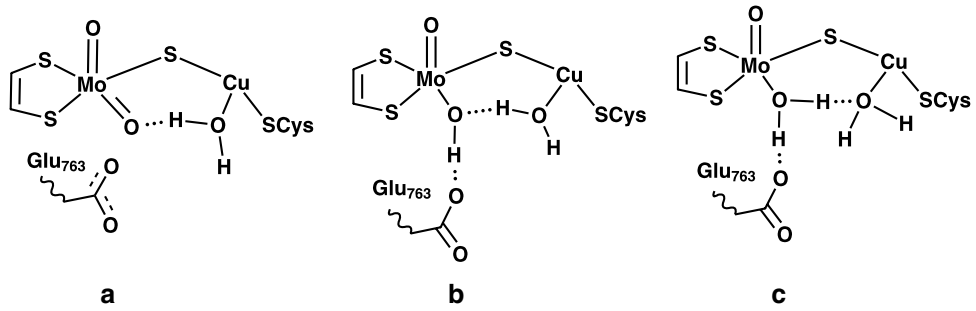


**Fig. 2** Schematic QM models with plausible equatorial ligands: **A** ($O^{2-}$), **B** ($OH^{-}$), and **C** ($H_2O$). The respective oxidation states of each model are as follows: **A1** and **A2** denote model **A** in the Mo(VI), and Mo(V) oxidation states, and **B1**, **B2**, and **B3** denote model **B** in the Mo(VI), Mo(V), and Mo(IV) oxidation states

calculated using the same level of theory as used for calculations of single point energy. Increased integration grids were used for the two metals to eliminate possible errors arising from numerical integration. The spin–orbit coupling operator was treated with an accurate spin–orbit mean-field (SOMF) approximation to the Breit–Pauli operator [25].

## Results and discussion

To understand structural variation arising from the variable protonation state of the Mo-coordinated equatorial oxygen ligand, as well as the role of catalytically important residues extending beyond the first coordination sphere, we postulate that a QM model is required that captures all key interactions that cumulatively tune the Mo–Cu site toward catalytic reactivity. Previous work investigating a large QM model of galactose oxidase revealed that the cumulative effect of weak, outer-sphere interactions is comparable in magnitude to those of the inner-sphere covalent/ionic interactions [26]. The absence of a proper model for the protein environment often results in theoretically unreasonable, non-analogous geometric and electronic structures of the bioinorganic active site.

### Structural parameters

We begin by analyzing structural data obtained from calculations in the oxidized state. Two possible protonation states of the Mo-coordinated water-derived equatorial ligand were considered: $O^{2-}$ in model **A1**, and $OH^-$ in model **B1** (Fig. 2), as these encompass both states proposed on the basis of experimental observation.

The optimized model **A1** ($Mo^{VI}$–$Cu^{I}$) exhibited structural features overall similar to those in the crystal structure with the exception of a more acute μS–Cu–$S_{Cys}$ bond angle relative to XRD data (calc.: 143°, XRD: 155°) (Table 1, relative RMSD in Table S1), though the calculated bond distances (contracted by ca. 0.04–0.06 Å) were qualitatively similar to those reported based on XRD. The Cu-coordinated water molecule was also found at a significantly shorter distance (calc.: 2.14 Å, XRD: 2.49 Å). This would be consistent with a particularly weak interaction between the water molecule and the metal center, potentially influenced by additional interactions within the active site. In contrast with EXAFS data, the two Mo–O bond distances were inequivalent (calc.: $Mo–O_{ax} = 1.73$ Å, $Mo–O_{eq} = 1.79$ Å), fully consistent with the elongated equatorial distance reported based on XRD.

In developing the model containing an equatorial $OH^-$ ligand coordinated to the Mo-center (model **B**), we initially considered structures arising from multiple possible hydrogen-bonding interactions between the equatorial ligand, Cu-coordinated water, and Glu763 (Fig. 3).

We found that the isomer in which the $OH^-$ ligand acts as a hydrogen-bond donor to the Cu-coordinated water molecule was higher in energy by approximately 7.5 kcal/mol than structures in which the equatorial ligand acts as a hydrogen-bond acceptor (Fig. 3). The highest energy structure (Fig. 3a) was considered no further for other oxidation states. Orienting the Cu-coordinated water as the hydrogen-bond donor directs the equatorial $OH^-$ proton toward Glu763. We have optimized both possible tautomeric forms, the proton residing on either the Mo-coordinated equatorial oxygen or the glutamic carboxylate of proximal Glu763. The latter, featuring a $MoO_2$-like core, (Fig. 3b) was approximately 3.3 kcal/mol lower in energy than the structure featuring equatorial $OH^-$ (Fig. 3c). The lowest energy model **B1** exhibited closer agreement with the XRD data than either conformation of the tautomer featuring equatorial $OH^-$ (RMSD in Table S1).

An overlay of the lowest energy model **B1** with the crystal coordinates is shown in Fig. 4, with a RMSD of 0.03 Å for bonds, and 3.0° for angles. In addition to some subtle changes at the core, we found that Phe390 in our models deviates from its crystallographic position. As noted previously, the position of the water molecule at the Cu-center in our models is controlled by a weak interaction with Phe390,

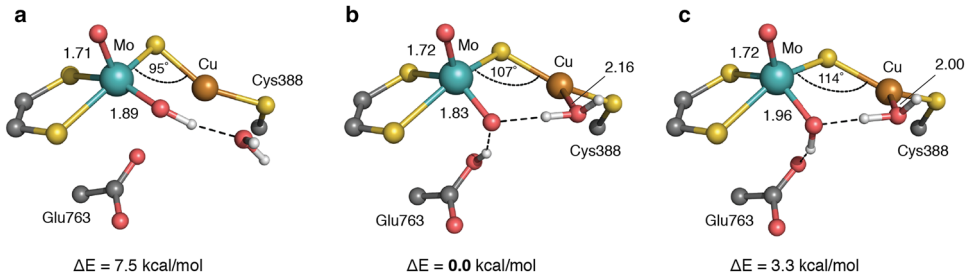


**Fig. 3** Optimized geometry of model **B1** for three possible hydrogen-bonding cases: **a** Cu-coordinated $H_2O$ as a proton acceptor from the equatorial $OH^-$, **b** and **c** Cu-coordinated $H_2O$ as a proton donor to the equatorial $OH^-$. Two tautomeric forms were optimized, with the proton residing on either the glutamate oxygen (**b**) or the equatorial oxygen (**c**) (Note: energies are reported relative to the structure shown in *panel b*; additional residues are omitted for clarity)

located in a flexible loop that extends from Cu-coordinated Cys388. As the position of Phe390 affects the nature of the Cu–$OH_2$ interaction, it is likely to influence substrate binding and product release as well. To achieve an energetically meaningful optimized structure and avoid unrealistic rigidity, no additional constraints were enforced for the structural stabilization of Phe390 during optimization.

Relative to the $Mo^{VI}$–$Cu^{I}$ oxidized state, several distinct changes were observed at the active site of the reduced enzymes in XRD and EXAFS, particularly in a few key distances and angles. The Mo···Cu and Mo–$O_{eq}$ distances were reported to increase by approximately 0.2 Å in XRD and 0.5 Å in EXAFS, whereas both key angles (Mo–μS–Cu, and μS–Cu–$S_{Cys}$) increased by approximately 5°–10°, rendering the μS–Cu–$S_{Cys}$ bond angle more obtuse than observed in the oxidized state (Table 1).

Starting from the structures optimized in the oxidized state, we subsequently optimized the corresponding two-electron reduced states including either a $OH^-$ (model **B3**) or $H_2O$ (model **C**) ligand at the Mo-equatorial position. Structural features calculated for both fully reduced models exhibited trends consistent overall with those reported by both EXAFS [5] and XRD [4]. The Mo···Cu and the Mo–$O_{eq}$ distances both increased by approximately 0.3 Å (Table 1). The distances and angles observed in the one-electron reduced models (**A2** and **B2**) are intermediate between those observed in the oxidized Mo(VI) and fully reduced Mo(IV) states.

We also employed a broken-symmetry approach to explore the anti-ferromagnetically coupled $Mo^{V}$–$Cu^{II}$ state, using the BP86 and B3LYP exchange-correlational functionals. All calculations invariably converged back to a closed-shell state featuring Mo(VI) and Cu(I). This result does not, however, exclude the existence of a broken-symmetry solution at some point during the catalytic cycle. This issue will require further investigation.

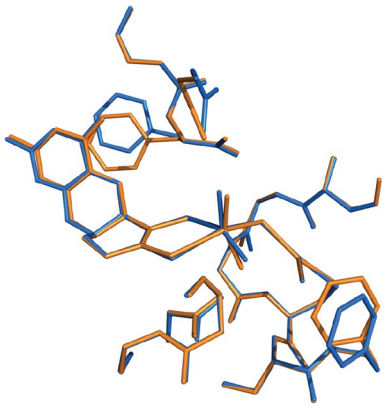

**Fig. 4** Overlay of the lowest energy optimized geometry of model **B1** with the initial crystal coordinates (*blue* crystal, *orange* optimized; RMSD: 0.42 Å for 98 heavy atoms (H atoms excluded), 0.03 Å for bonds, and 3.0° for angles)

## Electronic structure

Upon structural analysis of the oxidized state, two optimized models featuring a $MoO_2$-like core exhibited close agreement with the XRD data: model **A1** and the lowest energy model **B1**. The electronic structures of these two models, as well as their corresponding one- and two-electron reduced states, are discussed briefly below. The oxidation states of the metal centers were determined by analysis of the intrinsic atomic orbitals, following localization of the

**Table 1** Internuclear distances (Å) and angles (°) for models in different redox states, including ligand variation at the Mo-equatorial position as shown in Fig. 2

| Models | Oxidation states | Mo··Cu | Mo–$O_{ax}$ | Mo–$O_{eq}$ | Cu··$OH_2$ | Mo··O (Glu763) | Mo–μS–Cu | μS–Cu–Sγ |
|---|---|---|---|---|---|---|---|---|
| XRD | Mo(VI) | 3.74 | 1.77 | 1.86 | 2.49 | 3.18 | 113 | 155 |
| EXAFS | Mo(VI) | 3.70 | 1.74 | 1.74 | | 3.45 | | |
| XRD | Mo(IV) | 3.94 | 1.75 | 2.03 | 2.64 | 3.32 | 122 | 160 |
| EXAFS | Mo(IV) | 4.23 | 1.70 | 2.16 | | 3.26 | | |
| **A1** | Mo(VI) | 3.64 | 1.73 | 1.79 | 2.14 | 3.25 | 109 | 143 |
| **A2** | Mo(V) | 3.84 | 1.74 | 1.87 | 2.23 | 3.39 | 115 | 153 |
| **B1** | Mo(VI)[a] | 3.59 | 1.72 | 1.83 | 2.16 | 3.05 | 107 | 148 |
| **B2** | Mo(V) | 3.85 | 1.72 | 2.02 | 2.31 | 3.23 | 118 | 158 |
| **B3** | Mo(IV) | 3.94 | 1.74 | 2.14 | 2.47 | 3.36 | 119 | 159 |
| **C** | Mo(IV) | 3.94 | 1.73 | 2.19 | 3.10 | 3.30 | 121 | 169 |

[a] The lowest energy optimized structure, model **B1**, contains an equatorial oxo ligand at the Mo-center and a protonated Glu763. Copper remains in the +1 oxidation state in all models

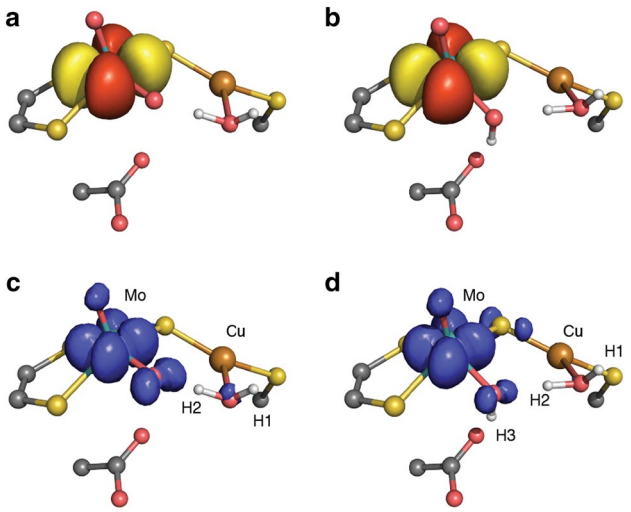


**Fig. 5** Molybdenum singly occupied intrinsic atomic 4*d* orbital (*top*) and spin density (*bottom*) plots for model **A2** (*left*) and model **B2** (*right*)

molecular orbitals using the approach suggested by Knizia [19]. A similar approach has been used recently to assign the oxidation state of the Mo-center in the FeMo cofactor of the nitrogenase enzyme [27]. Taking the sum of the occupancies of the orbitals strongly localized at the Cu-center, we have obtained an electron count that is consistent with a Cu(I) oxidation state (~28 $e^-$), regardless of the model analyzed (i.e., independent of the assigned oxidation states of Mo). For Mo, we have obtained a different picture, wherein each subsequent one-electron reduction of the system results in an increased number of electrons assigned to this center. For the oxidized model, we have obtained a small occupancy for the Mo 4*d*-orbitals (<0.2 $e^-$) indicative of a Mo(VI) oxidation state. Upon one-electron reduction of the model, we obtained an occupancy close to unity for one of the 4*d* orbitals of the Mo-center. As can be seen from Fig. 5, the shape of the orbital, which we have labeled '$d_{xy}$', is consistent with the spin density plot of this paramagnetic state. Following the second one-electron reduction, the electron count in the 4*d*-shell of Mo increases to ~1.8 $e^-$, in agreement with a Mo(IV) oxidation state (Fig. S1).

As mentioned above, parallels can be drawn between the localized Mo 4*d*-orbitals of the one-electron reduced models. In both cases, the unpaired electron was calculated to be localized primarily on the Mo-center (0.82 $e^-$ in model **A2**, 0.87 $e^-$ in model **B2**). The models varied, however, in the degree of delocalization via the μ-S bridge onto the Cu-center (μS = 0.01 $e^-$, Cu = 0.05 $e^-$ for model **A2** and μS = 0.05 $e^-$, Cu = 0.07 $e^-$ for model **B2**) (Fig. 5). Spin populations on the equatorial oxygen also differed considerably between the two models (0.12 $e^-$ for model **A2** and 0.05 $e^-$ for model **B2**). The calculated spin populations are in general agreement with those obtained for a synthetic analog of the active site, with the exception of an approximately threefold increase in the population on the bridging sulfur [28]. This difference could result from a primarily N-coordinated Mo-center in the synthetic complex.

**Table 2** Isotropic *g* values and hyperfine coupling constants (MHz) of one-electron reduced states

| | *g* | $A_{Mo}$ | $A_{Cu}$ |
|---|---|---|---|
| **A2** | 1.963 | 111 | 171 |
| **B2** | 1.979 | 114 | 306 |
| Exp.[a] | 1.972 | | 138 |
| Exp.[b] | 1.973 | | 202 |
| Synthetic model | 1.952 | 128 | 146 |
| Exp.[c] | 1.94 | 119 | 159 |

[a] CO reduced enzyme [29]

[b] Dithionite reduced enzyme in the presence of 100 mM bicarbonate [29]

[c] Synthetic model complex [28]

## Spectroscopic characterization

EPR and ENDOR have been used previously to probe the ligand environment in the Mo(V) state [4, 7], providing information related to the protonation state of the equatorial oxygen ligand and the spin density distribution in the paramagnetic state. It is expected that the differences in spin populations observed between the two models would be likewise reflected in their spectroscopic properties. Indeed, the computed g-tensors and $^{95}$Mo HFCs for **A2** and **B2** are in close agreement with the experimental data reported for the one-electron reduced enzymes and synthetic model (Table 2). Nevertheless, our calculations resulted in substantially different $^{63}$Cu HFCs between the two models. Strong variations in the $^{63}$Cu HFCs with respect to variations in structural parameters were observed in a previous theoretical study as well [28]. It is notable that the small model used in this previous study required the Mo–μS–Cu angle to be fixed at the crystallographic value to obtain $^{63}$Cu HFC consistent with experiment. In our model, this is not required, and our results indicate that a $MoO_2$-like core is in better agreement with the experimental results. Slight changes in the Mo–μS–Cu or μS–Cu–$S_{cys}$ bond angle are perhaps responsible for substantially different $^{63}$Cu HFC in the model containing an equatorial $OH^-$ ligand.

Furthermore, the proton hyperfine couplings (H1, H2, and H3 in Fig. 5) of the Cu-coordinated $H_2O$ and of the equatorial $OH^-$ at the Mo-center were found to be small, in the range of 1–3 MHz. In comparison, the g-tensor and HFC of a $MoO_2$-like core in the Mo(V) state are close,

within reason, to the data observed experimentally for the dithionite- and $H_2$-reduced forms of the enzyme [29], consistent with a similar Mo-core in the oxidized Mo(VI) state.

The calculated vibrational frequencies for both models (**A1** and **B1**) exhibit two distinct stretching frequencies corresponding to the axial (899 $cm^{-1}$ for model **A1**, 906 $cm^{-1}$ for model **B1**) and equatorial (776 $cm^{-1}$ for model **A1**, 702 $cm^{-1}$ for model **B1**) Mo–O bonds. The equatorial Mo–O modes exhibit far smaller displacement vectors relative to those of the axial species, and overlap with additional vibrational frequencies as well (Figs. S2–S3). In our model, the equatorial oxygen forms several H-bonding interactions with the Cu-coordinated water, Glu763, and the backbone N–H of Gly569. The absence of such extensive interactions involving the axial oxygen renders the two oxo ligands mutually distinct, thereby decoupling their respective vibrational stretching modes. The axial vibrational frequencies are comparable to the measured symmetric vibrational frequencies of the $MoO_2$ core (exp.: 895 $cm^{-1}$). Experimentally, an asymmetric vibrational mode was reported for the enzymes around 850 $cm^{-1}$ [6]. Our models also exhibited vibrational modes near 850 $cm^{-1}$ (Figs. S2–S3), which corresponded to a rocking motion of the N–H and O–H bonds that form hydrogen-bonding interactions with the Mo-equatorial oxygen.

## Electrochemical properties

We have used our models to evaluate electrochemical properties for all plausible redox couples. The reduction potentials of each Mo(VI)/Mo(IV) redox couple were investigated against the two-electron reduction potential for the catalytically active enzyme (ca. −558 mV at pH 7.0) [3]. The calculated reduction potentials were evaluated using a wide range of static dielectric constants to approximate a proper solvation environment around the active site. Although the calculated reduction potentials exhibited an expected dependence on the dielectric environment, only one of the redox couples (model **B1** with an equatorial oxo ligand and protonated Glu763, coupled with model **C** with an equatorial water) exhibited a reduction potential (calc.: −467 mV with $\varepsilon = 10$) in the ballpark of the experimental value (exp.: −558 mV). All other protonation states yielded reduction potentials that deviated greatly from experiment. For comparison, fixing the dielectric constant at $\varepsilon = 10$, all other possible redox couples yielded reduction potentials that varied on the order of ±500 to 1000 mV relative to the experimental value (Table 3). It is possible that Glu763 is deprotonated at some point during the substrate oxidation or reductive half-cycle of the enzyme, perhaps in conjunction with an electron transfer event. Our findings support the presence of a $MoO_2$-like core, with a protonated Glu763 in the catalytically active oxidized Mo(VI) state, and equatorial coordination by $H_2O$ in the fully reduced Mo(IV) state. This assignment is supportive of our initial postulate based on structural and spectroscopic comparisons.

**Table 3** Two-electron reduction potentials as a function of protonation state, with implicit solvent polarity indicated by the static dielectric constant ($\varepsilon$) ($E_{H+} = -0.42$ eV from water [24], Exp. = –558 mV [3])

| $\varepsilon$ | $E_{red}$ (V) | | | |
|---|---|---|---|---|
| | **B1** $\downarrow 2e^-$ **B3** | **A1** $\downarrow 2e^- + H^+$ **B3** | **B1** $\downarrow 2e^- + H^+$ **C** | **A1** $\downarrow 2e^- + 2H^+$ **C** |
| 4 | −3.074 | −1.754 | −0.939 | 0.381 |
| 10 | −1.913 | −1.074 | −0.467 | 0.372 |
| 15 | −1.629 | −0.907 | −0.352 | 0.370 |
| 20 | −1.483 | −0.821 | −0.293 | 0.369 |
| 80 | −1.143 | −0.622 | −0.155 | 0.366 |

## Impact of specific amino acids

Finally, to address the influence of the protein environment surrounding the Mo–Cu center, we have also explored geometric changes at the active site resulting from the removal of specific residues from the oxidized models (**A1**, and the two lowest energy tautomers of **B1**). For models featuring a $MoO_2$ core (**A1** and the lowest energy **B1**), removal of Glu763 had only a minor effect on structural parameters, attributable to an absence of hydrogen-bonding interaction with the equatorial oxygen. The absence of Val384-Arg387 and Phe390 led to smaller deviations in the Mo–Cu distance (reduced by ~0.1 to 0.2 Å), but resulted in a modest alteration of key bond angles (RMSD = ~7° to 9° for angles) (Tables S2–S3). It is interesting to note that the removal of Glu763 alone in model **B1** (containing equatorial $OH^-$, Fig. 3c) altered the Mo···Cu distance and the Mo–μS–Cu angle substantially (Table 4). This would suggest that Glu763 is relatively important when a protic ligand resides at the Mo-equatorial position. As Glu763 acts as a proton acceptor and is proposed to activate the equatorially coordinated water molecule, it would indeed appear to constitute an important residue for generating the $MoO_2$-like core for the oxidative half-reaction of the enzyme. All other truncations exhibited minimal structural effects, leading generally to slightly collapsed bond angles (RMSD = 3.5° for Val384–Arg387, and 2.6° for Ser570). Although removal of Ser570 led to no substantial structural alteration of the core, the proximity of Ser570 could potentially alter the proton donor–acceptor properties, and thereby, the protonation state and nucleophilicity of the Mo-coordinated equatorial oxygen ligand. This would require further evaluation in future studies.

**Table 4** Structural deviations in internuclear distances (Å) and angles (°) in the absence of particular residues from model **B1** with an equatorial hydroxo ligand

| | **B1** | Residues excluded | | | |
|---|---|---|---|---|---|
| | | Val384-Arg387 | Glu763 | Phe390 | Ser570 |
| Mo···Cu | 3.79 | −0.09 | −0.81 | 0.03 | −0.06 |
| Mo–$O_{ax}$ | 1.72 | 0 | 0 | 0 | 0 |
| Mo–$O_{eq}$ | 1.96 | 0.02 | 0.03 | 0.02 | −0.03 |
| Mo–S3(MCD) | 2.38 | 0.16 | 0.07 | −0.04 | 0.06 |
| Mo–S4(MCD) | 2.52 | −0.13 | −0.11 | −0.01 | −0.02 |
| Mo–μS | 2.26 | −0.02 | 0.02 | −0.01 | 0.01 |
| μS–Cu | 2.27 | −0.01 | −0.14 | 0.03 | −0.02 |
| Cu–$S_{Cys}$ | 2.16 | −0.01 | 0.02 | −0.02 | 0 |
| Cu···$OH_2$ | 2.00 | 0.02 | 0.16 | 0 | 0.03 |
| Mo–Oε(Glu763) | 3.08 | −0.04 | | 0.01 | 0.03 |
| Mo–μS–Cu | 114 | −3 | −29 | 0 | −2 |
| μS–Cu–$S_{Cys}$ | 135 | −4 | −1 | −2 | 3 |
| RMSD (bonds) | | 0.07 | 0.27 | 0.02 | 0.03 |
| RMSD (angles) | | 3.5 | 20.5 | 1.4 | 2.6 |

## Conclusions

We report here a realistic QM model developed for the bimetallic active site of CODH, including residues from the first and outer coordination spheres necessary to accurately reproduce experimentally determined structural parameters and structurally essential weak interactions surrounding the Mo–Cu core. We have explored all plausible protonation states of the Mo-equatorial oxygen ligand ($O^{2-}$, $OH^-$, and $H_2O$), as well as all catalytically plausible redox states ($Mo^{VI}$–$Cu^{I}$, $Mo^{V}$–$Cu^{II}$, $Mo^{V}$–$Cu^{I}$, and $Mo^{IV}$–$Cu^{I}$). We present a refined computational model for the oxidized state, and our data are in support of a model **B1**, in which Glu763 acts as an active site base, leading to a $MoO_2$-like core and a protonated Glu763. It is important to note that the calculations based on a $MoO_2$-like core are in better agreement with the structural parameters deduced from XRD experiment than with those derived from an EXAFS analysis [4, 5]. The two-electron reduced state led to optimized structures exhibiting structural changes similar to those reported previously based on both XRD and EXAFS.

The calculated electronic structure of the Mo(V) state supports some degree of delocalization across the Mo–μS–Cu core, which was found to vary with the protonation state of the Mo-equatorial ligand. In line with recent ENDOR [7], our investigations of hyperfine coupling also support a $MoO_2$-like core at the bimetallic center.

Our oxidized model featuring this $MoO_2$-like core produces Mo=$O_{ax}$ vibrational frequencies (906 $cm^{-1}$ for model **B1**) comparable to the experimentally observed Mo=O stretching mode reported for the enzyme at 895 $cm^{-1}$. The model also exhibits vibrations in the region previously assigned to a Mo=O asymmetric stretch (exp.: 861 $cm^{-1}$), though these correspond to a rocking motion of the N–H and O–H bonds that form hydrogen-bonding interactions with the Mo-equatorial oxygen (Figs. S2–S3) [6].

Based on the calculated two-electron reduction potentials for each plausible redox couple, we conclude that the redox couple formed by the lowest energy model **B1** in conjunction with model **C** is the only couple consistent with the experimental reduction potential. The reduction potentials calculated for all other redox couples deviated substantially from the reported experimental value (exp.: −558 mV). Removal of specific amino acids from our optimized model substantiated the postulated roles of Phe390, Glu763, and the flexible loop extending from Val384 through Arg387 as crucial to maintaining the essential structural features of the enzyme. Removal of Glu763 led to the greatest structural deviations when the Mo-equatorial ligand was a hydroxo in model **B1**. Our findings further support the previously suggested role of Glu763 as an active site proton acceptor [8], and better inform our understanding of the numerous weak interactions that enable catalytic activity at the unique Mo–Cu core.

In summary, our results suggest that substrate binds to an active site featuring a $MoO_2$-like core. The proton on the glutamic acid can subsequently undergo transfer to bulk solution or to other proton acceptors (e.g., MCD followed by FAD) before ultimately being shuttled out of the enzyme. The substrate- and various product-bound states involving Mo(V) are crucial to understanding the mechanism of catalysis, and it is essential to thoroughly investigate these intermediate complexes, using our computational model to gain further insight into the catalytic mechanism of CO oxidation in CODH.

**Acknowledgments** This research was funded by generous financial contributions from Whitman College and the M. J. Murdock Charitable Trust. Special thanks to Dr. Robert Szilagyi (Montana State University, Bozeman, MT) for his tremendous assistance in setting up the computational server at Whitman College, and for providing comments and feedback during the preparation of this manuscript. We gratefully acknowledge the Max Planck Society for financial support of this work.

## References

1. Mörsdorf G, Frunzke K, Gadkari D, Meyer O (1992) Biodegradation 3:61–82
2. Moxley JM, Smith KA (1998) Soil Biol Biochem 30:65–79
3. Wilcoxen J, Hille R (2013) J Biol Chem 288:36052–36060
4. Dobbek H, Gremer L, Kiefersauer R, Huber R, Meyer O (2002) Proc Natl Acad Sci 99:15971–15976
5. Gnida M, Ferner R, Gremer L, Meyer O, Meyer-Klaucke W (2003) Biochemistry 42:222–230

6. Zhang B, Hemann CF, Hille R (2010) J Biol Chem 285:12571–12578
7. Shanmugam M, Wilcoxen J, Habel-Rodriguez D, Cutsail GE 3rd, Kirk ML, Hoffman BM, Hille R (2013) J Am Chem Soc 135:17775–17782
8. Siegbahn PE, Shestakov AF (2005) J Comput Chem 26:888–898
9. Stein BW, Kirk ML (2015) J Biol Inorg Chem 20:183–194
10. Neese F (2012) Wiley Interdiscip Rev Comput Mol Sci 2:73–78
11. Klamt A, Schuurmann G (1993) J Chem Soc Perkin Trans 2:799–805
12. Becke AD (1988) Phys Rev A 38:3098–3100
13. Perdew JP (1986) Phys Rev B 33:8822–8824
14. Bühl M, Kabrede H (2006) J Chem Theory Comput 2:1282–1290
15. Pantazis DA, Chen X-Y, Landis CR, Neese F (2008) J Chem Theory Comput 4:908–919
16. Neese F (2003) J Comput Chem 24:1740–1747
17. Weigend F (2006) Phys Chem Chem Phys 8:1057–1065
18. Bykov D, Petrenko T, Izsák R, Kossmann S, Becker U, Valeev E, Neese F (2015) Mol Phys 113:1961–1977
19. Knizia G (2013) J Chem Theory Comput 9:4834–4843
20. Becke AD (1993) J Chem Phys 98:5648–5652
21. Staroverov VN, Scuseria GE, Tao J, Perdew JP (2003) J Chem Phys 119:12129–12137
22. Izsak R, Neese F (2011) J Chem Phys 135:144105
23. Neese F, Wennmohs F, Hansen A, Becker U (2009) Chem Phys 356:98–109
24. Palascak MW, Shields GC (2004) J Phys Chem A 108:3692–3694
25. Sinnecker S, Neese F (2006) J Comput Chem 27:1463–1475
26. Rokhsana D, Dooley DM, Szilagyi RK (2008) J Biol Inorg Chem 13:371–383
27. Bjornsson R, Lima FA, Spatzal T, Weyhermuller T, Glatzel P, Bill E, Einsle O, Neese F, DeBeer S (2014) Chem Sci 5:3096–3103
28. Gourlay C, Nielsen DJ, White JM, Knottenbelt SZ, Kirk ML, Young CG (2006) J Am Chem Soc 128:2164–2165
29. Hille R, Dingwall S, Wilcoxen J (2015) J Biol Inorg Chem 20:243–251